Dalton Transactions

PAPER

View Article Online
View Journal

Cite this: DOI: 10.1039/c5dt02905h

Synthesis, cytotoxicity and anti-cancer activity of new alkynyl-gold(I) complexes†

Assunta De Nisi,[a] Christian Bergamini,[b] Marco Leonzio,[a] Giorgio Sartor,[b] Romana Fato,[b] Marina Naldi,[b] Magda Monari,*[a] Natalia Calonghi*[b] and Marco Bandini*[a]

Received 28th July 2015,
Accepted 8th December 2015

DOI: 10.1039/c5dt02905h

www.rsc.org/dalton

Alkynyl(triphenylphosphine)gold(I) complexes carrying variously substituted propargylic amines have been synthesized and fully characterized in solution and solid state. High levels of toxicity (*i.e.* micromolar range) were recognized for a series of cancer cell lines with particular emphasis on HT29, IGROV1, HL60 and I407. In particular the lead compound **3ab** was identified as the most active compound in all cell lines (IC_{50}: 1.7–7.9 μM).

Introduction

The class of metallodrugs based on gold complexes continues to gain credit within the scientific community due to their consolidated multiple pharmacological activities.[1] In particular, seminal discoveries focusing on the treatment of symptoms of rheumatoid arthritis[2] were expanded by applications of gold complexes as antimalarial agents[3] and most recently also as anticancer drugs.[4]

The high toxicity that some gold(I), gold(III)[5] and gold nanoparticles[6]/nanorods[7] have shown against several tumour cell lines inspired the development of a number of structurally different organometallic species with chemical permutations both in the metal oxidation state and in the organic counterparts.[8]

In particular, the organic frameworks constituting the prodrug system proved to be actively involved in determining the overall toxicity of the species.[9] In this direction, soft ligands such as phosphines, thiols (class-I polymeric thiolates, class-II monomeric thiolates)[2] or σ-donating nitrogen heterocyclic carbenes (NHCs)[10] have been employed in gold complexes featuring anticancer activity.

Mechanistically, although, the real target of gold-based organometallic species is still under debate, recent investigations have unveiled that the observed cytotoxicity is mediated by their ability to alter mitochondrial functions through peculiar interactions with Se-containing enzymes TrxR.[11] This class of enzymes is involved in the defence against oxidative damage and in redox signalling. A growing number of transcription factors including NF-kappaB or the Ref-1-dependent AP1 require thioredoxin reduction for DNA binding.[12] Moreover, recent studies have shown that the antiproliferative properties of gold(I) and gold(III) adducts may include their interaction with DNA: as a matter of fact, rapid inhibition of DNA synthesis was observed for gold(I) complexes containing AMPP, dppe or ADPP ligands.[13]

Very recently, Ott and coworkers documented on the synthesis, characterization and pharmacological investigation of a new family of mononuclear [alkynyl(triphenylphosphine)gold(I)] complexes of general structure $PPh_3Au\text{-}C{\equiv}CCH_2XR$ (X: O, N) with important antiproliferative activity (micromolar range) in breast adenocarcinoma and colon carcinoma cells.[14a] Shortly after, the same team described the remarkable biological properties of binuclear gold(I) alkynyl analogs featuring bidentate phosphines as tethering units (Fig. 1).[14b] These studies emphasized also thioredoxin reductase (TrxR)[15] as a plausible biological target of the pharmacologically active gold(I) species.[16]

The propargylic sidearm proved to contribute substantially to the overall pharmacological activity of the title species, therefore, careful modulation of this unit could lead to interesting perspectives in developing more selective and potent candidates for anticancer drugs.

In this regard, we present our recent investigation dealing with the documentation of novel [alkynyl(triphenylphosphine)-gold(I)] complexes comprising relatively unexplored propargylic amine derivatives as organic ligands. The possibility to create chemical diversity by means of readily accessible propargylic

[a]*Department of Chemistry "G. Ciamician", Alma Mater Studiorum – University of Bologna, Via Selmi 2, 40126 Bologna, Italy. E-mail: marco.bandini@unibo.it; Fax: +39-051-2099456*

[b]*Department of Pharmacy and Biotechnology, Alma Mater Studiorum – University of Bologna, Via Irnerio 48, 40126 Bologna, Italy*

† Electronic supplementary information (ESI) available. CCDC 1045016 (**3ab**) and 1045017 (**3ac**). For ESI and crystallographic data in CIF or other electronic format see DOI: 10.1039/c5dt02905h

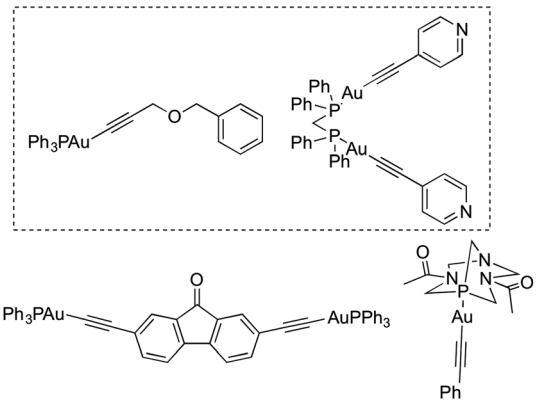

Fig. 1 Collection of reported [alkynyl(phosphine)gold(I)] complexes featuring antitumor activity.

amine derivatives enabled a survey of several structural aspects such as nitrogen basicity and electronic/steric factors.

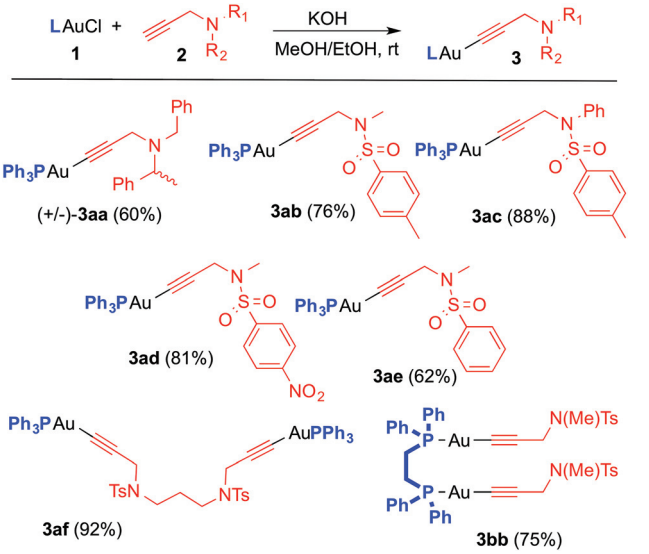

Scheme 1 Library of [gold(I)-alkynyl] complexes synthesized and tested in the present work. In the brackets: the isolated yields.

Results and discussion

Synthesis and characterization

In order to assess the effective role of the alkynyl sidearm in the biological spectrum of the gold species, a range of propargylic mono- and diamine derivatives **2a–f** and mono/binuclear phosphinogold(I) complexes (*i.e.* PPh_3AuCl **1a** and $[PPh_2(CH_2)_2PPh_2](AuCl)_2$ **1b**),[17] were selected as the key building blocks (Chart 1).

In particular, by reacting an equimolar amount of gold(I) chloride complexes **1a,b** and the desired terminal alkyne under basic conditions (KOH, MeOH/EtOH), the corresponding alkynyl-gold complexes **3** were isolated in moderate to good yields (60–92%). Further purification was commonly carried out either by recrystallization or through flash chromatography on silica gel (Scheme 1).

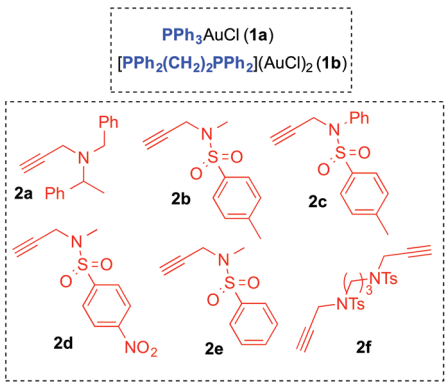

Chart 1 Metal and organic fragments employed in the present investigation.

Complexes **3** were obtained as white (pale brown in the case of **3ad**) air stable solids featuring remarkable solubility in common organic solvents. They were fully characterized both in solution (NMR, IR, LC-MS) and in the solid state (**3ab** and **3ac**).

In particular, NMR spectroscopy ($CDCl_3$, rt) was particularly diagnostic in monitoring the reaction course. As a matter of fact, the formation of adducts **3** caused the disappearance of the acetylenic C–H of the alkyne congeners (^{1}H-NMR δ = 2.0–2.2 ppm), with the concomitant deshielding (≈0.15 ppm) of the propargylic methylene. Additionally, a marked downshielding of the ^{31}P-NMR signals in the final compounds **3a–e** (39–42 ppm) occurred with respect to the congener **1a** (32.9 ppm). In contrast, the ^{31}P-NMR spectrum of the binuclear adduct **3bb** displayed a shielded singlet (δ = 21.8 ppm) when compared with **1b** (δ = 31.5 ppm). The presence of a single peak accounted for the formation of the C_2-symmetric adduct depicted in Scheme 1.

Solid state structure elucidation for complexes **3ab** and **3ac** was also carried out. In detail, crystals suitable for X-ray diffraction were collected through slow evaporation of EtOAc solutions of the corresponding species and the resulting structures are reported in Fig. 2.[18] As expected for gold(I) complexes, Au adopts an almost linear coordination and the P–Au–C bond angles are very close to the ideal 180° [176.5(2) and 178.9(2)° for **3ab** and **3ac**, respectively]. The C≡C bond lengths of 1.183(7) and 1.194(7) Å are typical of terminal alkynyl gold(I) complexes. The crystal packing of **3ab** is dominated by weak non-classical intermolecular C–H···O hydrogen bonds whereas in **3ac** two phosphine phenyl rings in each molecule establish intermolecular π–π interactions with their symmetrically equivalent adjacent phenyl ligands generating infinite zig-zag chains along the *c* axis (Fig. S1 and S2†).

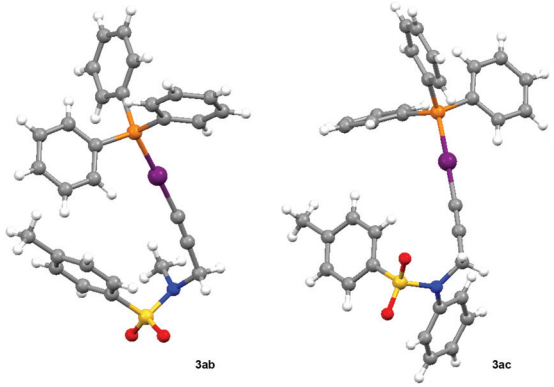

Fig. 2 Molecular structures of **3ab** (left) and **3ac** (right).

Biology

Cell lines included in the evaluation of toxicity profiles were malignant HT29, IGROV1, and HL60, and a non-malignant human epithelial intestinal cell line I407. IC_{50} values of the drugs were calculated using Prisma, fitted by means of sigmoidal fit and listed in Table 1.

From the data collected in Table 1 some preliminary conclusions can be drawn. Within the portfolio of gold complexes in hand, **3ab** was the more effective in inhibiting cell growth in all panel cell lines, auranofin, an antiarthritic gold(I) complex with antitumor activity, was included in the test panel for comparison.[19,20] Additionally, also compound **3ad** showed some levels of cytotoxicity towards all the cell lines but the corresponding IC_{50} values were constantly higher than that **3ab**. In contrast, (+/−)-**3aa**, **3ac**, **3bb**, **3ae** and **3af** proved competent only on a few of the screened cell lines. In this scenario some peculiarities were also highlighted. In particular, complexes **3af** and **3bb** showed significant toxicity for IGROV1 and HL60 cells, respectively. Additionally, it is important to stress the lack of toxicity toward non-cancer cell lines shown by compounds **3bb**, **3ae** and **3af**.

These bio-divergences clearly emphasised the role played by the presence of different moieties on the nitrogen atom in modulating the overall pharmacological properties of the gold complexes.

As mentioned above, inhibition of the seleno enzyme thioredoxin reductase (TrxR) is considered to be an important mechanism of the bioactivity of the gold(I) species.[21] In particular auranofin shows an high inhibitory effect both on cytosolic (TrxR1) and mitochondrial (TrxR2) isoforms of this enzyme.[22] Therefore, the potential of gold complexes to inhibit TrxR was studied on commercially available TrxR using the 2,6-dichloroindophenol (DCIP) reduction assay.

According to the results given in Table 2, complexes **3bb** and **3af** turned out to be effective inhibitors of TrxR showing an inhibitory potency close to that induced by auranofin with IC_{50} values in the sub-micromolar range. The other complexes showed IC_{50} values at least two orders of magnitude higher than the auranofin, whereas **3ab** cannot be considered an inhibitor of this class of enzymes.

It can be pointed out that only binuclear compounds are able to inhibit TrxR at sub-micromolar concentration suggesting the presence of strong interaction with the enzyme. To highlight the interaction between compounds and TrxR we have evaluated the LC-MS spectra of the enzyme both in the presence of a binuclear compound (**3bb**) and in the presence of the mononuclear compound **3ab** that does not inhibit the enzyme activity.

The results, reported in the ESI,† indicate that no covalent bond exists between TrxR and **3ab** or **3bb** (Fig. S3 and S4†).

Table 2 Inhibition power of gold(I) complexes on TrxR in comparison with auranofin[a]

Compound	% Of auranofin inhibition	IC_{50} (μM)
Auranofin	100	0.018
3bb	73	0.354
3af	73	0.308
3ae	52	1.555
3ad	55	3.754
3aa	33	0.818
3ab	—	—

[a] First column: the inhibitory effect of different gold(I) complexes on TrxR is expressed as % of inhibition taking as reference the auranofin maximal inhibition. Second column: IC_{50} values of the different gold(I) complexes and auranofin on TrxR activity.

Table 1 Half maximal inhibitory concentration (IC_{50}) of gold compounds in different cell lines after 24 h treatment (μM)[a]

Compound	HT29	IGROV1	HL60	I407
Auranofin	3.3 (1.8–6)	2.5 (0.4–15)	0.7 (0.3–1.6)	1.6 (0.9–2.8)
(+/−)-**3aa**	>100	20 (10.06–39.20)	19.0 (7.43–50.69)	15.0 (9.14–24.65)
3ab	7.9 (5.39–11.59)	5.3 (3.87–7.43)	3.3 (1.62–6.88)	1.7 (0.61–4.99)
3ac	>100	5.5 (4.69–6–69)	2.7 (1.19–6.18)	9.6 (7.26–12.63)
3ad	11.0 (8.97–15.01)	6.5 (4.12–10.31)	6.3 (5.05–7.94)	8.0 (6.73–9.66)
3ae	>100	10.0 (6.40–17.84)	9.0 (6.55–12.83)	>100
3af	>100	7.7 (6.26–9.48)	>100	>100
3bb	>100	>100	0.8 (0.28–2.40)	>100

[a] 95% confidence intervals are reported in the brackets.

To gain some insight into the biological effects of these new derivatives, the most active compound toward all cell lines, **3ab** was subjected to additional studies. In order to assess whether its effect was due to interference with cell cycle progression, DNA profiles of cultured cells were examined by flow cytometry and cell cycle analysis was performed by using the Multicycle Cycle Phoenix Flow system, and Modfit 5.0 software. Table 3 shows that the treatment with **3ab** caused a marked accumulation of HT29, IGROV1 and I407 cells in the S phase, with respect to untreated cells.

In contrast, in HL60 treated cells, the growth arrest in the G0/G1 phase of the cell cycle was associated with a well distinguishable pre-G1 peak in DNA, suggestive of DNA fragmentation, characteristic of apoptosis (Fig. 3).

Interestingly, the treatment with the binuclear compounds did not induce any effect on the cell cycle, as reported in Table 4, where the cell cycle distribution of IGROV1 and HL60 in the presence of **3af** and **3bb**, respectively is shown.

UV-Vis absorption titration analysis

Interactions between small molecules and DNA rank among the primary action mechanisms of cytotoxic activity. In order to compare the binding properties of the gold complexes with DNA, dissociation constants (K_d) were determined through inverse titration experiments. Two types of interactions can be devised by these experiments as we can argue by either an increase or a decrease of ΔA measured at 260 nm.

Table 3 Cell cycle distribution of cell lines treated with **3ab**

	G0/G1 %	S %	G2/M %
HT29	49.05	39.58	11.37
HT29 + **3ab** (7.9 μM)	45.72	45.25	9.03
IGROV1	55.32	29.57	15.11
IGROV1 + **3ab** (5.3 μM)	50.71	37.16	12.13
I407	70.38	23.62	6
I407 + **3ab** (1.7 μM)	62.64	28.52	8.84

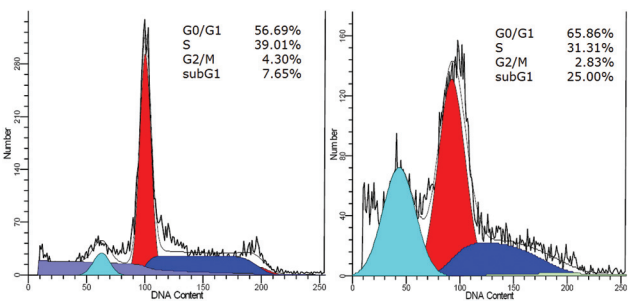

Fig. 3 Effect of compound **3ab** on the HL60 cell cycle. The cells were incubated for 24 h, (sx) with the vehicle (Ctrl), or (dx) with compound **3ab** (3.3 μM), afterwards cell cycle distribution was determined by flow cytometry. Following treatment with **3ab**, the cells are in the G0/G1 phase and a well detectable fraction of DNA is present as a sub-G1 peak (light blue peak).

Table 4 Cell cycle distribution of cell lines treated with **3af** and **3bb**

	G0/G1 %	S %	G2/M %
IGROV1	60	25	15
IGROV1 + **3af** (7.7 μM)	64	23	13
HL60	48	14	38
HL60 + **3bb** (0.8 μM)	50	17	33

The increase of differential absorption of DNA in the presence of **3af**, **3ab**, **3ac**, **3bb**, and **3ac** can be ascribed to a lower base stacking while the decreased differential absorbance observed for (+/−)-**3aa** suggests a higher compactness of DNA. No appreciable effect was observed for **3ad**. In this regard, the differential spectra of **3af** (A), (+/−)-**3aa** (B) and **3ad** (C) are depicted in Fig. 4.

We then plot the differential absorbance at 260 nm for each molecule *versus* DNA concentration, as reported in Fig. 5.

The estimation of the dissociation constant (K_d) for the complex formation as well as the limiting value for the ΔA_{260} was obtained fitting these data using a one-site saturation equation (Table 5).

The K_d analysis confirms that **3ab** interacts with DNA quite strongly (K_d = 0.84 ± 0.17 μM) suggesting a partial explanation for its cellular toxicity. Among the other compounds, only **3af** shows a strong interaction with DNA having a similar value of K_d (1.54 ± 0.58 μM). On the other hand, a decrease for the differential absorption spectra is observed for (+/−)-**3aa**. While the increase in the absorbance at 260 nm can be ascribed to a partial DNA denaturation, the decrease observed in the presence of compound **3aa**, could be indicative of DNA supercoiling.

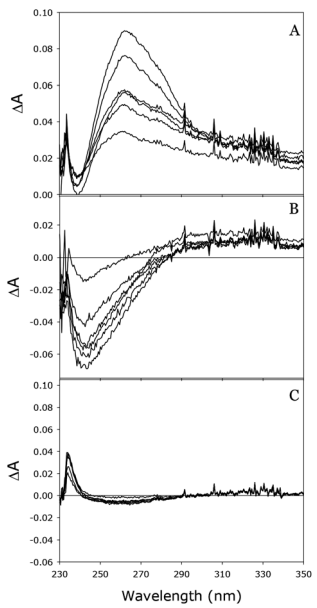

Fig. 4 Differential absorption spectra of **3af** (A), (+/−)-**3aa** (B) and **3ad** (C) titrated with DNA.

Fluorescence titration of 15 μM ETBr bound to DNA with **3ab**, up to 200 μM, does not show any appreciable change of the emission spectra of ETBr, suggesting that no intercalation of **3ab** with DNA takes place (Fig. 6).

Conclusions

In conclusion, a new class of neutral [Au(I)]-alkynyl complexes based on monodentate or bidentate phosphine ligands has been developed and fully characterized both in the liquid and solid state. The gold(I)–C_{sp} linkage was efficiently realized in high yields (60–92%) by condensing the gold-chloride congener with pre-functionalized terminal alkynes under convenient mild conditions (KOH, MeOH/EtOH).

Additionally, the biological activity of these organometallic species was comprehensively investigated and the data reported suggest that their cellular toxicity could be related to different mechanisms acting on different biological targets.

Compound **3ab** showed a marked cytotoxicity on all cell lines tested, with IC_{50} values ranging from 1.7 μM for I407 to 7.9 μM for HT29 and caused cell cycle arrest in the S phase. Only in the HL60 cell line the growth arrest was in the G0/G1 phase of the cell cycle and it was associated with a well distinguishable pre-G1 peak that indicates DNA fragmentation that is characteristic of apoptosis. These effects on the cell cycle can be associated with an interaction of the molecule with DNA and this hypothesis is supported by the results of DNA titration where the dissociation constant of **3ab** with salmon sperm DNA is in the sub-micromolar range. The real mechanism of **3ab**–DNA interaction has not yet been fully elucidated, however, it cannot be attributed to an intercalation of the molecule into the DNA helix. Additionally, it should be mentioned that **3ab** does not show any inhibitory effect on the thioredoxin reductase enzymatic activity.

On the other hand, the binuclear compounds (**3bb** and **3af**) showed a cytotoxic effect only in HL60 (**3bb**: IC_{50} = 0.8 μM) and in IGROV1 (**3af**: IC_{50} = 7.7 μM) and they do not show any effect on the cell cycle (Table 4). This evidence suggests that the biological target of binuclear gold-species is not the DNA and they appear to act through the inhibition of thioredoxin reductase at sub-micromolar concentration (Table 2). However the mechanism of interaction of our alkynyl-gold(I) complexes with thioredoxin reductase is different as compared to auranofin and other gold compounds.[23] In fact, while auranofin induces a mass shift in the mass spectra of this enzyme suggestive of protein binding of the gold-containing molecule,[22] in our study no covalent adducts with the enzyme have been detected using LC/ESI-MS (see ESI†).

Moreover, inhibition of thioredoxin reductase is responsible for a decrease of the oxidative stress resistance and for alterations in redox signalling that are key factors for cell survival. Cancer cells are more resistant toward oxidative stress, for this reason compounds that are able to interfer with this phenomena, have a good chance to be anticancer drug candidates. Studies addressing the clarification and/or identification of additional biological targets as well as the development of structure–activity relationships are currently ongoing in our laboratories.

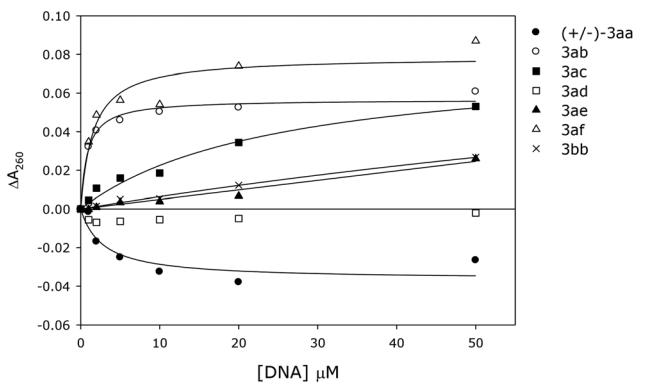

Fig. 5 Differential absorbance at 260 nm of DNA–molecule complexes at increasing DNA concentration. Molecule concentration was 10 μM.

Table 5 Dissociation constant for the complex formation and the limiting value for the ΔA_{260} obtained by fitting data in Fig. 5

Compound	K_d ± SE (μM)	B_{max} ± SE	r^2
(+/−)-**3aa**	2.78 ± 1.63	−0.0366 ± 0.0055	0.8564
3ab	0.84 ± 0.17	0.0568 ± 0.0019	0.9826
3ac	24.89 ± 7.12	0.0784 ± 0.0108	0.9757
3bb	195.53 ± 111.89	0.1310 ± 0.0619	0.9923
3ad	—	—	—
3ac	—	—	—
3af	1.54 ± 0.58	0.0786 ± 0.0064	0.9245

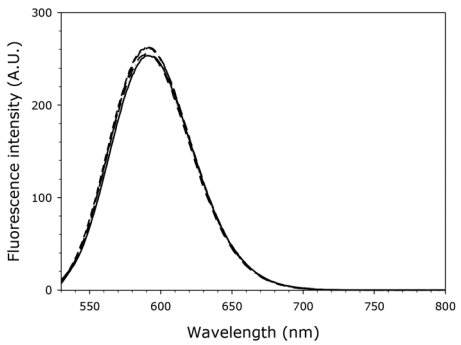

Fig. 6 Fluorescence emission spectra of 15 μM ETBr bound to DNA in the presence of increasing concentration of **3ab**. Control: solid line; [**3ab**] 10 μM: long dashed line; [**3ab**] 50 μM: short dashed line; [**3ab**] 100 μM: dashed dotted line; [**3ab**] 200 μM: dotted line.

Experimental

Synthesis of the nitrogen containing [alkynylAu(I)] complexes 3

A solution of the desired alkyne (1.2 or 2.4 eq.) in reagent grade MeOH/EtOH (1 : 1 ratio, 0.05 M) was treated with the

desired gold(I)chloride precursor (**1a,b**, 1 eq.) and a solution of KOH (4 eq., 2 M in MeOH). The mixture was stirred in the dark until complete consumption of the alkyne. The resulting solid was collected by filtration and washed with cooled MeOH. Pure material can be obtained *via* re-crystallization from a DCM : pentane solution, or flash chromatography.

(+/−)-**3aa**: white solid, purification *via* flash chromatography (cHex : AcOEt = 9 : 1–7 : 3); yield = 60%; 85–86 °C; IR = 2159 cm^{-1} (C≡C); ^{1}H-NMR (400 MHz, $CDCl_3$): δ 1.44 (d, J(H,H) = 6.4 Hz, 3H); 3.40 (d, J(H,H) = 17.6 Hz, 1H); 3.61 (d, J(H,H) = 2.0 Hz, 2H); 3.68 (d, J(H,H) = 17.6 Hz, 1H); 4.00 (q, J(H,H) = 6.4 Hz, 1H); 7.24–7.52 (m, 25H); ^{13}C-NMR (100 MHz, $CDCl_3$): δ 21.4, 39.5, 54.3, 60.5, 98.0, 98.2, 124.3, 126.5, 126.6, 126.9, 127.6, 128.0, 128.2, 128.4, 128.9, 129.0, 129.1, 129.7, 130.2, 131.5, 132.5, 134.3, 134.4, 140.2, 146.2; ^{31}P-NMR (162 MHz, $CDCl_3$): δ = 42.0 (br s) ppm; ESI Q-TOF for ($C_{36}H_{33}AuNP$: 707.2016), (m/z): 708.2090 ($M + H^+$).

3ab: white solid; yield = 76%; mp = 175–177 °C; IR = 2137 cm^{-1} (C≡C); ^{1}H-NMR (400 MHz, $CDCl_3$): δ = 2.29 (s, 3H); 2.86 (s, 3H); 4.08 (s, 2H); 7.25 (d, J(H,H) = 7.2 Hz, 2H); 7.44 (m, 15H); 7.73 (d, J(H,H) = 7.2 Hz, 2H); ^{13}C-NMR (100 MHz, $CDCl_3$, diagnostic signals): δ = 21.4, 34.2, 41.0, 95.4, 95.6, 128.1, 129.1, 129.2, 129.4, 129.9, 131.6, 134.2, 134.3, 143.1; ^{31}P-NMR (162 MHz, $CDCl_3$): δ = 41.9 (br s) ppm; LC/MS-ESI (m/z): ESI Q-TOF for ($C_{29}H_{27}AuNO_2PS$: 681.1196), (m/z): 682.1244 ($M + H^+$).

3ac: white solid; yield = 88%; mp = 139–141 °C; IR = 2134 cm^{-1} (C≡C); ^{1}H-NMR (400 MHz, $CDCl_3$): δ = 2.32 (br s, 3H); 4.61 (s, 2H); 7.17 (d, J(H,H) = 8.4 Hz, 2H); 7.26–7.35 (m, 2H); 7.37–7.38 (m, 2H), 7.44–7.54 (m, 16H), 7.64 (d, J(H,H) = 8.4 Hz, 2H); ^{13}C-NMR (100 MHz, $CDCl_3$, diagnostic signals): δ = 21.5, 42.2, 127.4, 128.2, 128.3, 128.8, 129.0, 129.1, 129.2, 130.0, 131.6, 134.2, 134.3, 136.0, 140.0, 142.9; ^{31}P-NMR (162 MHz, $CDCl_3$): δ = 42.4 (s) ppm; ESI Q-TOF for ($C_{34}H_{29}AuNO_2PS$: 743.1322), (m/z): 766.1220 ($M + Na^+$).

3ad: pale yellow solid; yield = 81%; mp = 208–210 °C; IR = 2137 cm^{-1} (C≡C); ^{1}H-NMR (400 MHz, $CDCl_3$): δ = 2.95 (s, 3H); 4.27 (d, J(H,H) = 1.6 Hz, 2H); 7.43–7.53 (m, 15H); 8.13 (d, J(H,H) = 8.8 Hz, 2H); 8.34 (d, J(H,H) = 8.8 Hz, 2H); ^{13}C-NMR (100 MHz, $CDCl_3$): δ = 34.4, 41.2, 93.7, 94.0, 123.9, 129.2, 129.6, 131.6, 134.0, 134.2, 143.8, 149.9; ^{31}P-NMR (162 MHz, $CDCl_3$): δ = 39.4 (s) ppm; ESI Q-TOF for ($C_{28}H_{24}AuN_2O_2PS$: 712.0860), (m/z): 713.0940 ($M + H^+$).

3ae: white solid; yield = 62%; mp = 210–212 °C; IR = 2136 cm^{-1} (C≡C); ^{1}H-NMR (400 MHz, $CDCl_3$): δ = 2.91 (s, 3H); 4.14 (s, 2H); 7.44–7.48 (m, 18H); 7.88 (d, J(H,H) = 6.8 Hz, 2H); ^{13}C-NMR (100 MHz, $CDCl_3$, diagnostic signals): δ = 34.3, 41.0, 95.3, 99.0, 127.8, 128.1, 128.7, 129.0, 129.1, 129.2, 129.4, 129.9, 131.6, 131.7, 132.4, 134.1, 134.3, 137.5; ^{31}P-NMR (162 MHz, $CDCl_3$): δ = 39.2 (s) ppm; ESI Q-TOF for ($C_{28}H_{25}AuNO_2PS$: 667.1009), (m/z): 668.1088 ($M + H^+$).

3af: pale yellow solid; yield = 92%; mp = decomposition; IR = 2132 cm^{-1} (C═C); ^{1}H-NMR (400 MHz, $CDCl_3$): δ = 1.97–1.98 (m, 2H), 2.24 (s, 6H), 3.37 (t, J(H,H) = 6.8 Hz, 4H), 4.29 (s, 4H), 7.22–7.29 (d, J(H,H) = 8.4 Hz, 4H), 7.45–7.56 (m, 30H), 7.81 (d, J(H,H) = 8.4 Hz, 4H); ^{13}C-NMR (100 MHz, $CDCl_3$, diagnostic signals): δ = 21.4, 25.8, 37.6, 43.7, 95.1, 127.7, 127.8, 127.9, 129.0, 129.1, 129.2, 129.4, 130.0, 131.4, 131.5, 134.1, 134.2, 136.1, 142.7; ^{31}P-NMR (162 MHz, $CDCl_3$): δ = 40.9 (br s); LC/MS-ESI (m/z): 1375 ($M + H^+$).

3bb: white solid; yield = 75%; IR = 2123 cm^{-1} (C≡C); ^{1}H-NMR (400 MHz, $CDCl_3$): δ = 1.70 (s, 1H), 2.31 (s, 6H); 2.86 (s, 6H); 4.05 (s, 4H); 7.26–7.72 (m, 30H); ^{13}C-NMR (100 MHz, CD_3CN, diagnostic signals): δ = 20.6, 33.5, 33.9, 40.9, 41.4, 77.6, 92.4, 127.8, 127.9, 128.9, 129.4, 129.5, 129.6, 130.4, 131.9, 132.2, 133.3, 133.4, 143.6; ^{31}P-NMR (162 MHz, $CDCl_3$): δ = 21.8 ppm.

Cell culture and cytotoxicity

Cell lines (HT29, IGROV1, HL60 and I407) were routinely cultured in RPMI 1640 medium (Lonza) supplemented with penicillin (Sigma-Aldrich) (100 U mL^{-1}), streptomycin (Sigma-Aldrich) (100 μg mL^{-1}), and 10% fetal bovine serum (Euroclone) in an environment of 5% CO_2, 37 °C and sub-cultured using a trypsin 0.25%–EDTA (Sigma-Aldrich) 0.02% solution. The cytotoxicity was determined with the MTT (3-(4,5-dimethylthiazol-2-yl)-2,5-diphenyltetrazolium bromide) (Sigma-Aldrich) dye reduction assay.

Cells were plated in 96-well flat-bottom microplates at a density of 1×10^5 cells per mL (100 μL per well), and 24 h later the test compounds were added, appropriately diluted with DMSO. The cells were exposed to various concentrations of the compounds (in a range 1 nM to 100 μM) for 24 h. The cytotoxicity was determined with the MTT (3-(4,5-dimethylthiazol-2-yl)-2,5-diphenyltetrazolium bromide) dye reduction assay with minor modifications.[20] Briefly, after incubation with the test compounds, MTT solution (0.2 mg mL^{-1} in PBS) was added (100 μL per well). The plates were further incubated for 2 h at 37 °C, and the formazan crystals formed were dissolved by adding 100 μL per well of propanol. Optical densitometry was determined with a Wallac 1420 Victor2 Microplate Reader (Perkin Elmer) at 570 nm.

One hundred microliters of culture medium supplemented with the same amount of MTT solution and solvent was used as the blank solution. The IC_{50} value was calculated according to the GraphPad Prism 5 software. All data are expressed as mean ± SD.

Cell cycle analysis

Cells were plated at an initial density of 10 000–20 000 cells per cm^2 in dish or flask, depending on the cell line. After 72 h of adhesion, the cells were treated with drugs at the concentration corresponding to the calculated IC_{50}, and after 24 h of treatment the effect was evaluated. Untreated and 24 h treated cells were detached, washed with PBS and the pellet was finally re-suspended in 0.01% Nonidet P-40 (Sigma-Aldrich), 10 μg per mL RNase (Sigma-Aldrich), 0.1% sodium citrate (Sigma-Aldrich), 50 μg per mL propidium iodide (PI) (Sigma-Aldrich), for 30 min at room temperature in the dark. Propidium iodide (PI) fluorescence was analyzed using a Beckman Coulter Epics XL-MCL flow cytometer and cell analysis was performed using the M cycle (Verity) and MODFIT 5.0 software.

TrxR inhibition assay

For this purpose, commercially available rat liver TrxR (Sigma-Aldrich) was used and diluted with distilled water to achieve a concentration of 0.05 U mL^{-1}. The gold(I) complexes were freshly dissolved as stock solutions in DMSO. The reduction of the DCIP (2,6-dichloroindophenol) was followed spectrophotometrically at 600 nm using ε = 19.1 mM cm^{-1} using a Jasco V-550 spectrophotometer equipped with a stirring device and thermostatic control.

To each cuvette was added: 100 μL of enzyme solution, different concentrations of the compounds (ranging from 1 to 100 μM) or vehicle, 100 μM DCIP, 8 mM EDTA, 0.001% BSA in 20 mM potassium phosphate buffer pH 7.1 ml final volume.

The reaction was started by the addition of 2 mM NADPH. The IC_{50} values were calculated as the concentration of compound required to decrease enzyme activity of the untreated control by 50%, and are given as the means ± SD of 3–6 independent experiments.

DNA–compound interaction assay

Absorption titration experiments were carried out by keeping constant the concentration of compounds (10 μM) while raising the DNA concentration from 1 μM to 50 μM ([DNA]/[compounds] ratio from 0.1 to 5) in buffer solution (BS; 50 mM NaCl, 5 mM TRIS buffer, pH 7.2) and 4% of DMSO. The UV-Vis spectra were obtained using a Jasco V-550 spectrophotometer. The absorbance spectra were obtained scanning the solution in 1 cm quartz cuvettes from 230 nm to 400 nm using 2 nm band width. The solubility of different compounds was checked evaluating the lack of scattering. Then additions of standard DNA were performed. After each addition of DNA the absorbance spectrum was recorded. The DNA stock solution was prepared with low molecular weight from salmon sperm, Sigma Aldrich in BS. The DNA stock solution concentration was determined spectrophotometrically (λ: 260 nm), using an extinction coefficient of 6600 M^{-1} cm^{-1}.

The blanks were prepared with standard DNA titration from 1 μM to 50 μM in BS and 4% of DMSO.

The UV-Vis spectra of DNA in the presence of the different compounds were obtained using a Jasco v-550 spectrophotometer (see ESI†). The data analysis was carried out on the subtracted spectrum (ΔA_λ): the spectra of titration experiments were subtracted by standard DNA titration and compound lacking DNA:

$$\Delta A_\lambda = (\Delta A_{\text{DNA–compound}})_\lambda - (\Delta A_{\text{DNA}})_\lambda - (\Delta A_{\text{compound}})_\lambda$$

The compounds' absorbance variations at 260 nm (ΔA_{260}) were plotted *versus* DNA concentration. The calculation of binding parameters was carried out fitting ΔA_{260} using the following equation:

$$\Delta A_{260} = \frac{B_{\max}[\text{DNA}]}{K_d + [\text{DNA}]}$$

where K_d represents the dissociated constant of DNA complex for every compound and $B_{\max}$ represents the limiting value of ΔA_{260}.

Competitive binding fluorescence studies

Aliquots of stock solution of the gold complex **3ab** dissolved in DMSO were added to solutions containing 15 μM calf thymus DNA (ctDNA) base pairs and 15 μM ethidium bromide (ETBr) in 15% DMSO 25 mM Tris-HCl buffer (pH 7.0) at 25 °C to give the final complex concentration ranging from 0 to 200 μM, according to the literature.[22,24] Excitation wavelength was set at 500 nm and emission spectra were recorded between 530 and 800 nm. Blank subtraction was applied.

Acknowledgements

Acknowledgements for funding are made to MIUR – Rome and the University of Bologna. We are also grateful to Si Hui Elisa Chen and Ciro Romano for the technical assistance and helpful discussion.

Notes and references

1 For a collection of recent reviews see: (*a*) C. F. Shaw III, *Chem. Rev.*, 1999, **99**, 2589–2600; (*b*) P. J. Barnard and S. J. Berners-Price, *Coord. Chem. Rev.*, 2007, **251**, 1889–1902; (*c*) I. Ott, *Coord. Chem. Rev.*, 2009, **253**, 1670–1681; (*d*) S. Nobili, E. Mini, I. Landini, C. Gabbiani, A. Casini and L. Messori, *Med. Res. Rev.*, 2010, **30**, 550–580; (*e*) S. J. Tan, Y. K. Yan, P. P. F. Lee and K. H. Lim, *Future Med. Chem.*, 2010, **2**, 1591–1608; (*f*) S. J. Berners-Prize, in *Bioinorganic Medicinal Chemistry*, ed. E. Alessio, Weinheim, 2011; (*g*) S. Komeda and A. Casini, *Curr. Top. Med. Chem.*, 2012, **12**, 219–235; (*h*) K. D. Mjos and C. Orvig, *Chem. Rev.*, 2014, **114**, 4540–4563.

2 The most recently introduced gold(I)-drug for treatment of the symptoms of rheumatoid arthritis is auranofin (commercial name Ridaura®) in 1985: (*a*) B. M. Sutton, E. McGusty, D. T. Walz and M. J. DiMartino, *J. Med. Chem.*, 1972, **15**, 1095–1098; (*b*) B. M. Sutton, *Gold Bull.*, 1986, **19**, 15–16.

3 For recent publications on the field see: (*a*) M. Altaf, M. Monim-ul-Mehboob, A. A. A. Seliman, M. Sohail, M. I. M. Wazeer, A. A. Isab, L. Li, V. Dhuna, G. Bhatia and K. Dhuna, *Eur. J. Med. Chem.*, 2015, **90**, 464–472; (*b*) L. Boselli, M. Carraz, S. Mazeres, L. Paloque, G. Gonzaĺez, F. Benoit-Vical, A. Valentin, C. Hemmert and H. Gornitzka, *Organometallics*, 2015, **34**, 1046–1055; (*c*) N. Pantelic, T. P. Stanojkovic, B. B. Zmejkovski, T. J. Sabo and G. N. Kaluderovic, *Eur. J. Med. Chem.*, 2015, **90**, 766–774; (*d*) T. Traut-Johnstone, S. Kanyanda, F. H. Kriel, T. Viljoen, P. D. R. Kotze, W. E. van Zyl, J. Coates, D. J. G. Rees, M. Meyer, R. Hewer, D. Bradley and G. Williams, *J. Inorg. Biochem.*, 2015, **145**, 108–120.

4 (*a*) M. Navarro, *Coord. Chem. Rev.*, 2009, **253**, 1619–1626; (*b*) J. Coetzee, S. Cronje, L. Dobrzanska, H. G. Raubenheimer, G. Joone, M. J. Nell and H. C. Hoppe, *Dalton Trans.*, 2011, **40**, 1471–1483.

5 For representative examples see: (*a*) P. I. da Silva Maia, V. M. Deflon and U. Abram, *Future Med. Chem.*, 2014, **6**, 1515–1536; (*b*) C. T. Lum, R. W.-Y. Sun, T. Zou and C.-M. Che, *Chem. Sci.*, 2014, **5**, 1579–1584.

6 (*a*) B. Kang, M. A. Mackey and M. A. El-Sayed, *J. Am. Chem. Soc.*, 2010, **132**, 1517–1519; (*b*) R. Geetha, T. Ashokkumar, S. Tamilselvan, K. Govindaraju, M. Sadiq and G. Singaravelu, *Cancer Nanotechnol.*, 2013, **4**, 91–98; (*c*) C. C. Chen, D. S. Hsieh, K. J. Huang, Y. L. Chan, P. D. Hong, M. K. Yeh and C. J. Wu, *Drug Des.*, 2014, **16**, 459–474; (*d*) U. Y. Lee, Y. S. Youn, J. Park and E. S. Lee, *ACS Nano*, 2014, **8**, 12858–12865.

7 R. Mooney, L. Roma, D. Zhao, D. Van Haute, E. Garcia, S. U. Kim, A. J. Annala, K. S. Aboody and J. M. Berlin, *ACS Nano*, 2014, **8**, 12450–12460.

8 C. Nardon, G. Boscutti and D. Fregona, *Anticancer Res.*, 2014, **34**, 487–492.

9 S. J. Berners-Price and P. J. Barnard, in *Ligand Design in Medicinal Inorganic Chemistry*, Wiley, 2014, pp. 227–256.

10 (*a*) L. Messori and C. Gabbiani, *Metals Compounds in Cancer Chemotherapy*, ed. J. M. Pérez, M. A. Fuertes and C. Alonso, Research Signpost, 2005, pp. 355–375; (*b*) S. Pengfei and J. Qin, *Prog. Chem.*, 2009, **21**, 644–653; (*c*) C. A. Tessier, C. L. Cannon and W. J. Youngs, *Chem. Rev.*, 2009, **109**, 3859–3884; (*d*) R. Rubbiani, S. Can, I. Kitanovic, H. Alborzinia, M. Stefanopoulou, M. Kokoschka, S. Mönchgesang, W. S. Sheldrick, S. Wölfl and I. Ott, *J. Med. Chem.*, 2011, **54**, 8646–8657; (*e*) W. Liu and R. Gust, *Chem. Soc. Rev.*, 2013, **42**, 755–773; (*f*) F. Cisnetti and A. Gautier, *Angew. Chem., Int. Ed.*, 2013, **52**, 11976–11978; (*g*) C. Hu, X. Li, W. Wang, R. Zhang and L. Deng, *Curr. Med. Chem.*, 2014, **21**, 1220–1230; (*h*) X. Cheng, P. Holenya, S. Can, H. Alborzinia, T. Rubbiani, I. Ott and S. Woelfl, *Mol. Cancer*, 2014, **13**, 221/1–221/15; (*i*) M. Tacke, *J. Organomet. Chem.*, 2015, **782**, 17–21; (*j*) E. Garcia-Moreno, S. Gascon, J. A. Garcia de Jalon, E. Romanos, M. J. Rodriguez-Yoldi and M. Laguna, *Anti-Cancer Agents Med. Chem.*, 2015, **10**, 773–782.

11 (*a*) I. Ott, *Coord. Chem. Rev.*, 2009, **253**, 1670–1681; (*b*) P. J. Barnard and S. J. Berners-Price, *Coord. Chem. Rev.*, 2007, **251**, 1889–1902; (*c*) C. Marzano, V. Gandin, A. Folda, G. Scutari, A. Bindoli and M. P. Rigobello, *Free Radicals Biol. Med.*, 2008, **42**, 872–881; (*d*) V. Gandin, A. P. Fernandes, M. P. Rigobello, B. Dani, F. Sorrentino, F. Tisato, M. Björnstedt, A. Bindoli, A. Sturaro, R. Rella and C. Marzano, *Biochem. Pharmacol.*, 2010, **15**, 90–101; (*e*) T. V. Serebryanskaya, A. S. Lyakhov, L. S. Ivashkevich, J. Schur, C. Frias, A. Prokop and I. Ott, *Dalton Trans.*, 2015, **44**, 1161–1169.

12 (*a*) E. S. Arner and A. Holmgren, *Eur. J. Biochem.*, 2000, **267**, 6102–6109; (*b*) L. Ortego, F. Cardoso, S. Martins, M. F. Fillat, A. Laguna, M. Meireles, M. D. Villacampa and M. C. Gimeno, *J. Inorg. Biochem.*, 2014, **130**, 32–37.

13 (*a*) S. J. Berners-Price, C. K. Mirabelli, R. K. Johnson, M. R. Mattern, F. L. McCabe, L. F. Faucette, C. M. Sung, S. M. Mong, P. J. Sadler and S. T. Crooke, *Cancer Res.*, 1986, **46**, 5486–5493; (*b*) M. J. McKeage, P. Papathanasiou, G. Salem, A. Sjaarda, G. F. Swiegers, P. Waring and S. B. Wild, *Metal-Based Drugs*, 1998, **5**, 217–223; (*c*) G. Lupidi, L. Avenali, M. Bramucci, L. Quassinti, R. Pettinari, H. K. Khalife, H. Gali-Muhtasib, F. Marchetti and C. Pettinari, *J. Inorg. Biochem.*, 2013, **124**, 78–87; (*d*) F. Kuralay and A. Erdem, *Analyst*, 2015, **140**, 2876–2880.

14 (*a*) A. Meyer, C. P. Bagowski, M. Kokoschka, M. Stefanopoulou, H. Alborzinia, S. Can, D. H. Vlecken, W. S. Sheldrick, S. Wölfl and I. Ott, *Angew. Chem.*, 2012, **124**, 9025–9030, (*Angew. Chem., Int. Ed.*, 2012, **51**, 8895–8899); (*b*) A. Meyer, A. Gutiérrez, I. Ott and L. Rodríguez, *Inorg. Chim. Acta*, 2013, **398**, 72–76.

15 See also: (*a*) E. Schuh, S. M. Validi, M. A. Jakupec, B. K. Keppler, P. Chiba and F. Mohr, *Dalton Trans.*, 2009, 10841–10845; (*b*) C. H. Chiu, R. S. M. Wong, R. Gambari, G. Y. M. Cheng, M. C. W. Yuen, K. W. Chan, S. W. Tong, F. Y. Lau, P. B. S. Lai, K. H. Lam, C. L. Ho, C. W. Kan, K. S. Y. Leung and W. Y. Wong, *Bioorg. Med. Chem.*, 2009, **17**, 7872–7877; (*c*) E. Vergara, E. Cerrada, A. Casini, O. Zava, M. Laguna and P. J. Dyson, *Organometallics*, 2010, **29**, 2596–2603; (*d*) R. G. Balasingham, C. F. Williams, H. J. Mottram, M. P. Coogan and S. J. A. Pope, *Organometallics*, 2012, **31**, 5835–5843.

16 (*a*) A. Bindoli, M. P. Rigobello, G. Scutari, C. Gabbiani, A. Casini and L. Messori, *Coord. Chem. Rev.*, 2009, **253**, 1692–1707; (*b*) A. de Almeida, D. E. Oliveira, J. D. G. Correia, G. Soveralc and A. Casini, *Coord. Chem. Rev.*, 2013, **257**, 2689–2704.

17 C. K. Mirabelli, D. T. Hill, L. F. Faucette, F. L. McCabe, G. R. Girard, D. B. Bryan, B. M. Sutton, J. O'Leary Bartus, S. T. Crooke and R. K. Johnsont, *J. Med. Chem.*, 1987, **30**, 2181–2190.

18 CCDC 1045016 (**3ab**) and 1045017 (**3ac**) contain the supplementary crystallographic data for this paper.

19 PPh_3 and **2b** were tested in the cell lines IGROV1 and HT29. Here, the alkyne proved to be inactive in both cases and the PPh_3 furnished the following IC_{50} values: 47 μM (IGROV1) and 39 μM (HT29).

20 C. K. Mirabelli, R. K. Johnson, C. M. Sung, L. Faucette, K. Muirhead and S. T. Crooke, *Cancer Res.*, 1985, **45**, 32–39.

21 I. Mickuviene, V. Kirveliene and B. Juodka, *Toxicol. In Vitro*, 2004, **18**, 639–648.

22 A. Casini, C. Gabbiani, F. Sorrentino, M. P. Rigobello, A. Bindoli, T. J. Geldbach, A. Marrone, N. Re, C. G. Hartinger, P. J. Dyson and L. Messori, *J. Med. Chem.*, 2008, **51**, 6773–6781.

23 K. J. Akerman, A. M. Fagenson, V. Cyril, M. Taylor, M. T. Muller, M. P. Akerman and O. Q. Munro, *J. Am. Chem. Soc.*, 2014, **136**, 5670–5682.

24 A. Albert, C. Brauckmann, F. Blaske, M. Sperling, C. Engelhard and U. Karst, *J. Anal. At. Spectrom.*, 2012, **27**, 975–981.

